

Nanoparticle Field Extraction Thruster (nanoFET): Introduction to, Analysis of, and Experimental Results from the “No-liquid” Configuration

AIAA-2008-5097

Louis Musinski^{*}, Thomas Liu[†], Inkyu Eu[‡], Brian Gilchrist[§], Alec Gallimore^{**},
Joanna Mirecki-Millunchick^{††}
University of Michigan, Ann Arbor, MI, 48109

David Morris^{‡‡}
ElectroDynamic Applications, Inc., Ann Arbor, MI, 48105

Abstract

This paper introduces a nanoparticle field extraction thruster (nanoFET) concept that does not depend on the liquid delivery of micro and nano-particles for extraction and acceleration. The no-liquid approach potentially provides important advantages such as allowing the use of smaller particles for propellant, which may offer a greater specific impulse. The most likely developmental obstacles are the adhesion of the particles to the source electrode and the cohesion between the particles. Adhesion and cohesion models are presented along with proposed methods of overcoming each.

A method of using the applied charging electric field to overcome the adhesion force is investigated, which predicts that it may be possible to remove particles with diameters down to hundreds or even tens of nanometers from a planar electrode with only the application of a high strength electric field. To investigate this particle removal model, eight test cases, involving 4 particle sizes and 2 electrode materials, are presented.

A method of transporting the dry particle propellant through an ultra-fine sieve prior to the charging and accelerating stages is investigated as a method of overcoming the cohesion between the particles. A simple proof-of-concept experiment is presented which indicates that this method is capable of breaking the cohesion force under appropriate conditions, which helps to guide future research.

Nomenclature

A	= Area [m ²]	h	= Lifshitz-van de Waals constant [J]
D	= Electrode gap [m]	r	= Particle radius [m]
d	= Particle diameter [m]	r_c	= Contact radius [m]
E	= Electric field [V/m]	ρ	= Particle mass density [kg/m ³]
ϵ	= Permittivity [F/m]	V	= Electric potential [V]
F	= Force on particle [N]	z	= Van der Waals separation [m]
g	= Gravitational acceleration [m/s ²]		

^{*} Graduate Student, Electrical Engineering, louisdm@umich.edu, AIAA Student Member

[†] Graduate Student, Aerospace Engineering, liutm@umich.edu, AIAA Student Member

[‡] Graduate Student, Material Science and Engineering, inkyu@umich.edu

[§] Professor, Electrical Engineering & Space Systems, gilchrst@umich.edu, AIAA Associate Fellow

^{**} Arthur F. Thurnau Professor, Aerospace Engineering & Applied Physics, rasta@umich.edu, AIAA Associate Fellow

^{††} Associate Professor, Material Science and Engineering, joannamm@umich.edu

^{‡‡} Senior Engineer, morris@edapplications.com, AIAA Member

1. Introduction

The nanoparticle field extraction thruster, nanoFET, is an electrostatic propulsion concept that utilizes micro- and nano-electromechanical systems (NEMS/MEMS) to transport, charge, and accelerate micro- and nano-particle propellant.^{1,2} The majority of research and development has focused on the insulating liquid design configuration shown in Figure 1.

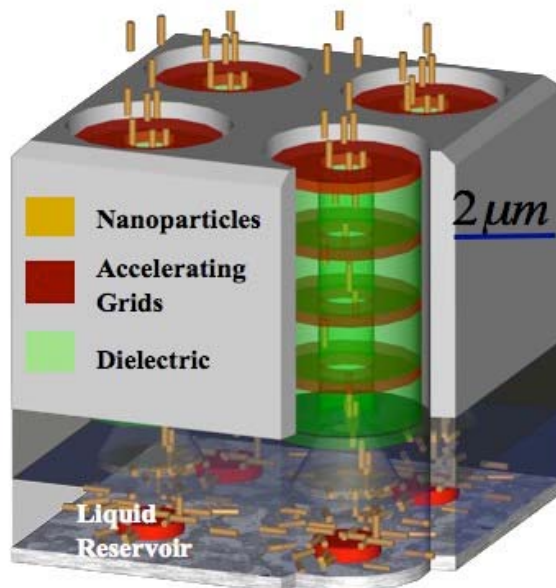


Figure 1: Schematic showing four emitters from the insulating liquid design configuration.

Figure 1 is a schematic of four emitters from the MEMS/NEMS based nanoFET thruster concept where a multi-layer grid establishes the critical electric fields to charge, extract, accelerate, and eject conducting micro- and nano-particles (one example shown in Figure 2)³ from the surface of an insulating liquid used to transport these particles. Note that the use of MEM/NEMS technologies are expected to allow large arrays to be fabricated with millions of emitters per square centimeter.

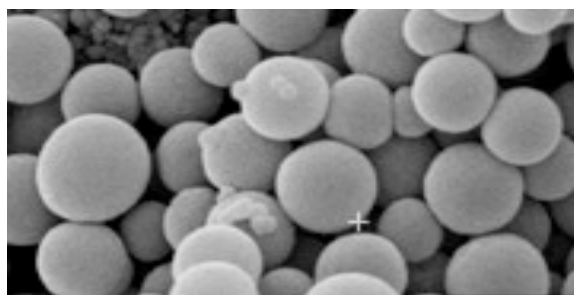


Figure 2: Example of a collection of unsorted nanoparticles in the 10 nm diameter range.

To understand how nanoFET's insulating liquid configuration works, Figure 3 depicts a model of a single emission zone. The particles are initially housed in a low vapor pressure liquid-filled storage reservoir. These spheres or cylinders are then transported through a microfluidic transport system to emission zones. These zones are comprised of multiple layers of stacked electrodes with millions of micron-sized channels for particle acceleration. Beneath the accelerating channels are electrical charging pads that are submersed in the low vapor pressure liquid. The layers of stacked electrodes and the charging pads are electrically biased to produce strong electric fields in the accelerating channels and within the liquid reservoir.

Particles delivered to the emission zones through the microfluidic transport system become electrically charged when they contact one of the charging pads. After acquiring sufficient charge, the particles are

transported by the electric field to the liquid surface, extracted through the surface, accelerated in the channels, and finally ejected to produce thrust.⁴

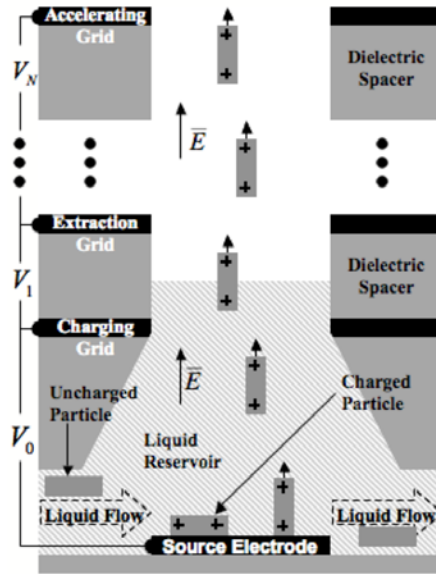


Figure 3: Cross-section of a single emission channel used with the insulating liquid configuration.

This paper presents a parallel design configuration that is being pursued that eliminates the use of the liquid, and instead transports, charges, and ejects dry micro- and nano-particles. The complete design of this system is beyond the scope of this paper, but will be presented in an upcoming publication. This paper refers to this design as the no-liquid configuration. Figure 4 is a preliminary illustration showing the delivery, charging, and acceleration stages of the no-liquid configuration, which uses a method of transporting the dry particle propellant through an ultra-fine *sieve* to separate the clumped nano-particle powder into individually isolated particles prior to charging and acceleration. The system consists of a particle storage reservoir directly against the ultra-fine sieve with a control piston that supplies pressure to help force the particles through the sieve, which is aided by a vibrational source (not shown). The sieve size is matched to the particle size so that only one particle is capable of passing through each sieve orifice at a time, which breaks the clumped powder into individually isolated particles. Above the sieve are the stacked charging and acceleration grids similar to the insulating liquid configuration. Electric potentials are applied across the conducting sieve and the stacked grids to generate the charging and accelerating electric fields used to charge and accelerate the individual particles that pass through the sieve.

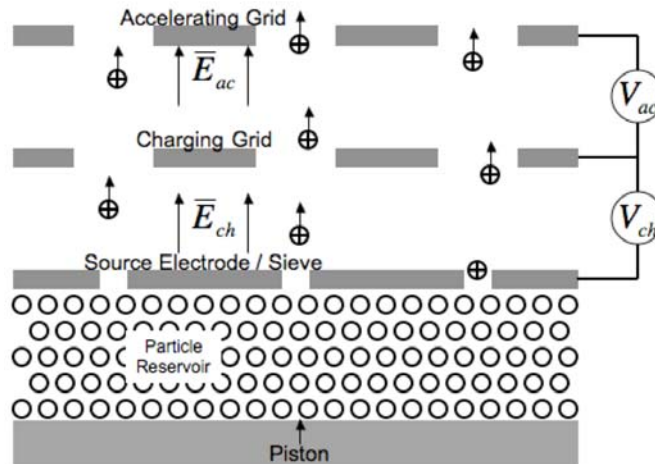


Figure 4: Sketch of a no-liquid configuration nanoFET concept. Dimensions are not to scale.

Previous studies working with nanometer and micron sized particles explain that particles on this size scale have a strong tendency to adhere to each other (*cohesion*) and to other objects that they contact (*adhesion*).⁵ Therefore, an understanding of the adhesion and cohesion forces and how to overcome them is extremely important to the development of the no-liquid configuration to assure that the particles do not clump together through cohesion or stick to the source electrode through adhesion. This paper presents a theoretical analysis of the adhesion and cohesion forces. In addition, the electric force arising from the charging electric field acting on the charged particles is investigated, both theoretically and experimentally, as a method to overcome the adhesion force and achieve particle removal from the source electrode. Finally a proof-of-concept experiment with the goal of demonstrating the feasibility of overcoming the cohesion force with the sieving particle delivery system is presented.

2. Adhesion and Cohesion Forces

There are four primary forces generally credited for the adhesion and cohesion of small particles.^{5,6} The relative magnitude of these forces is dependent on the size of the particles, the materials involved, and the environmental conditions. The most dominant of these forces when considering dry, conducting particles smaller than several hundred microns is the van der Waals force.

The van der Waals force between atoms arises when an apolar atom momentarily has a dipole moment due to the movement of its electrons with respect to its nucleus. This momentary dipole creates an electric field, which induces dipole moments in neighboring atoms. The resulting dipoles attract each other as the positive end of one atom aligns with the negative end of another.⁵

The van der Waals force between macroscopic bodies is calculated by taking the summation of the van der Waals forces between the atoms of the different bodies. The van der Waals force density between two infinite parallel planar surfaces is calculated to be dependent on the Lifshitz-van der Waals constant, h , and the separation between the surfaces, z .⁵

$$\frac{F_{vdw}}{A} = \frac{h}{8\pi^2 z^3} \quad (1)$$

The Lifshitz-van der Waals constant has units of energy and is a function of the material combination involved. The values for select materials are published, but are disputed by many authors, which is briefly discussed in Section 3. It is accepted that typical values of the Lifshitz-van der Waals constant range from 0.6 to 9.0 eV.⁶ According to Curran, a minimum separation distance of 4 Angstroms is acceptable when evaluating the van der Waals force.⁷

Using the van der Waals force density between two parallel planar surfaces given in Equation (1), the adhesion force between a spherical particle and an infinite planar surface (Equation (2)) and the cohesion force between two spherical particles (Equation (3)) are calculated.⁵

$$F_{vdw-ad} \approx \frac{hr}{8\pi z^2} \quad (2)$$

$$F_{vdw-co} \approx \frac{hr}{16\pi z^2} \quad (3)$$

The simple expressions for the adhesion and cohesion van der Waals forces scale directly with the particles' radii and inversely with the square of the minimum separation.

A comparison of the van der Waals forces reveals that the adhesion and cohesion forces scale the same with the particle size, but the adhesion force is approximately twice the cohesion force when using particles of the same size. Figure 5 is a plot of the adhesion and cohesion forces as a function of particle diameter when using a Lifshitz-van der Waals constant of 9 eV. For comparison purposes, the weight of the particle is included in the plot when the particle is made from aluminum.

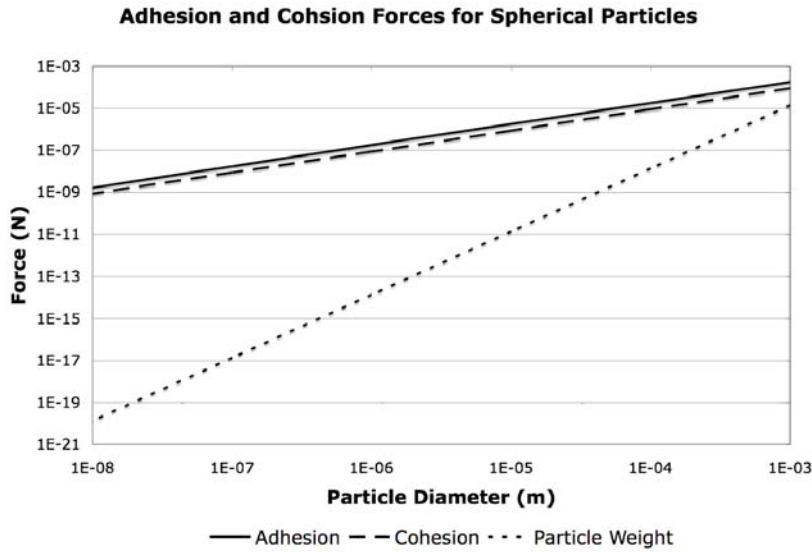


Figure 5: Plot of the adhesion and cohesion forces using a Lifshitz-van der Waals constant of 9 eV, and the weight of an aluminum particle.

The plot in Figure 5 shows that as the particle size decreases, the adhesion and cohesion forces decrease. This is somewhat misleading because, by comparison to the gravitational force, both the adhesion and cohesion forces become more significant for smaller particles.

3. Overcoming the Adhesion Force Using High Strength Electric Fields

The removal of micro- and nano-particles from surfaces is important to many applications, particularly in the MEMS and pharmaceutical industries. A few techniques currently used for particle removal are ultrasonic vibration, mechanical vibration, and laser irradiation.^{5,8} These techniques work by accelerating the particles relative to the surface. This section investigates an alternative method of particle removal using high strength electric fields, which lends itself nicely to the design of micro- and nano-particle thrusters, which use high strength electric fields to charge the particles when they are in contact with the source electrode. This section presents the electric force on a spherical conducting particle when in contact with an infinite planar electrode and applies this force to determine the required electric field to overcome the van der Waals adhesion force.

The model for spherical particle removal from a planar electrode is shown in Figure 6 and consists of two infinite parallel electrodes with a conducting spherical particle in contact with the upper surface of the bottom electrode. An electric potential bias, V , is applied across the electrodes to generate an electric field within the gap.

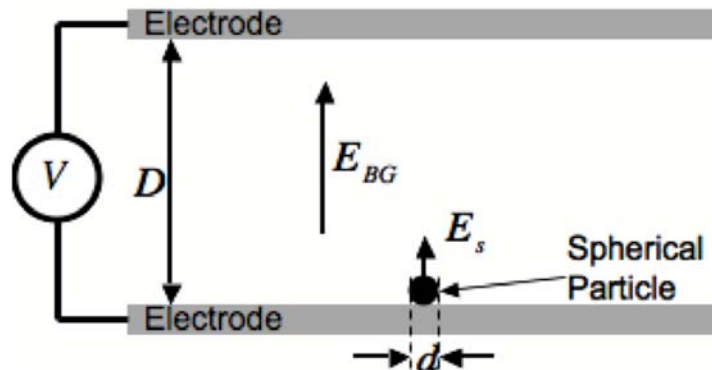


Figure 6: Model for the removal of a conducting spherical particle from a planar electrode using a high strength electric field.

The complete derivation of the electric force on the spherical particle when in contact with the source electrode is beyond the scope of this paper. Felici calculated it when assuming the particle is much smaller than the electrode gap ($d \ll D$).^{9,10}

$$F_{el} \approx 5.5\pi r^2 \epsilon E_{BG}^2 \quad (4)$$

Using the model for the electric force on a conducting particle in contact with the source electrode from Equation (4) and the van der Waals adhesion force from Equation (2), the threshold background electric field for particle removal can be calculated when the van der Waals force is dominant. It is important to include the gravitational force on the particle in this calculation to show where the adhesion force becomes more important than gravity.

$$F_g = \frac{4}{3}\pi r^3 \rho g \quad (5)$$

By combining Equations (2), (4), and (5), the threshold background electric field for overcoming the adhesion force is determined when the particle is much smaller than the electrode gap.

$$E_{thresh} \approx \sqrt{\frac{1}{r} \frac{h}{z^2 \epsilon} (0.0023) + r \frac{\rho g}{\epsilon} (0.24)} \quad (6)$$

It is important to note that the threshold electric field can be broken down into two terms: the adhesion dominant term and the gravitational dominant term. The adhesion dominant term scales inversely with the square root of the particle size while the gravitational term scales directly with the square root of the particle size.

Figure 7 is a plot of the predicted threshold electric field for overcoming the van der Waals adhesion force and the gravitational force for the two cases when the Lifshitz-van der Waals constant is 9 eV and 0.6 eV. The particle density is assumed to be 1,000 kg/m³ and the surrounding medium is vacuum.

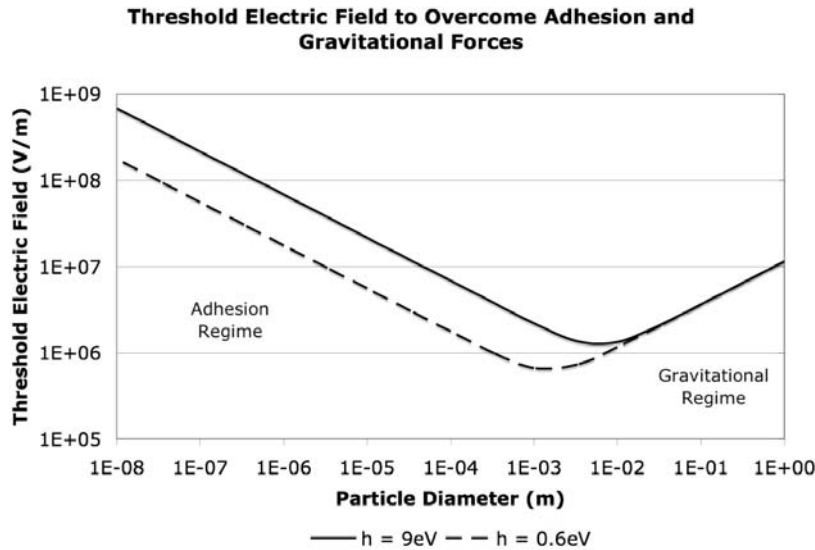


Figure 7: Plot of the threshold electric field to overcome the adhesion and gravitational forces holding a spherical particle in contact with the source electrode.

The plot of the threshold electric field clearly illustrates the two regimes. Particles much larger than the centimeter range lie within the gravitational regime and particles much smaller than millimeter range lie within the adhesion regime. Both forces affect particles between these two ranges significantly. According to the plot, it may be possible to remove spherical particles with diameters as small as tens of nanometers when keeping the background electric field less than approximately 100 MV/m, which is approximately one order of magnitude less than required for electron emission.¹¹

A. Experimental Setup

To experimentally investigate the van der Waals adhesion force and to overcome this force by way of an electric force, the system depicted in Figure 8 was constructed, which is very similar to the model in Figure 6 with the addition of the thin strip of Kapton® tape over the surface of the upper electrode. Note that the Kapton® tape does modify the background electric field slightly, which is taken into account in the results section.

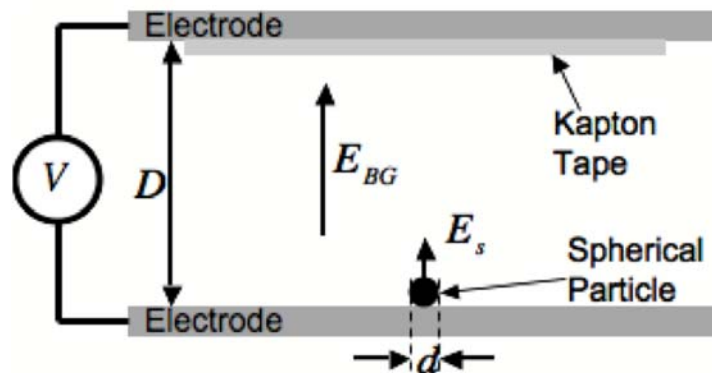


Figure 8: Depiction of the experimental setup used for investigating the adhesion force and using an electric force to overcome this adhesion force.

The goals of the experiment are to measure the threshold electric field required for removing conducting spherical particles from the electrode surface for various particles in the adhesion dominant regime, investigate the effects of particle size on the adhesion force, and investigate the effects of the particle and electrode materials on the adhesion force.

The experiment is performed by depositing approximately 100 conducting spherical micro-particles on the surface of the bottom electrode. To prevent the particles from clumping together through cohesion, the particles are passed through a micro-sieve to separate the clumps into individual particles prior to deposition onto the electrode surface. It is desirable to have the particles separated by a distance of at least ten times their diameter to ensure that neighboring particles do not affect the electric field profile at their surfaces. Once the particles are deposited, the upper electrode is secured in place to provide the correct uniform electrode gap, which is regulated by a spacer, either 1.0 mm or 4.0 mm thick. Next, the voltage across the electrodes is increased incrementally to generate the strong electric field within the gap. At each voltage increment, a photograph of the particles remaining in contact with the source electrode is taken to provide visual evidence of the number of particles removed. The process is repeated until all of the particles have been removed. Finally, the number of particles removed from the electrode surface at each voltage increment is counted, providing an experimental measurement of the threshold electric field required for particle removal.

The particles removed from the source electrode during testing are accelerated across the electrode gap towards the upper electrode and onto the Kapton® tape, where they remain trapped. The Kapton® tape serves to collect the removed particles so that they do not oscillate between the electrodes and disrupt the particles still adhered to the bottom electrode. The tape used for this experiment had a thickness of approximately 25 µm and Kapton® typically has a relative dielectric constant of approximately 2.7.¹²

The experiment was performed with four different spherical particle sizes, ranging in diameter from 53 microns to 305 microns, which are all in the adhesion dominant regime. Table 1 lists the mean diameters, tolerances, materials, densities, and manufacturers of the particles.

Mean Diameter (µm)	Tolerance (±µm)	Material Composition	Density (kg/m ³)	Manufacturer
305	10	95%Sn / 5%Sb	7,250	Indium Corp
196	16	Soda-lime glass coated w/ Ag	2,500	Mo-Sci Corp
102	10	95%Sn / 5%Sb	7,250	Indium Corp
53	4	Soda-lime glass coated w/ Ag	2,500	Mo-Sci Corp

Table 1: Properties of the four particles used in the particle adhesion experiment.

Figure 9 is a set of photographs of the four particles and includes a close-up shot and a distance shot of each particle size. These photographs were taken using a scanning electron microscope (SEM).

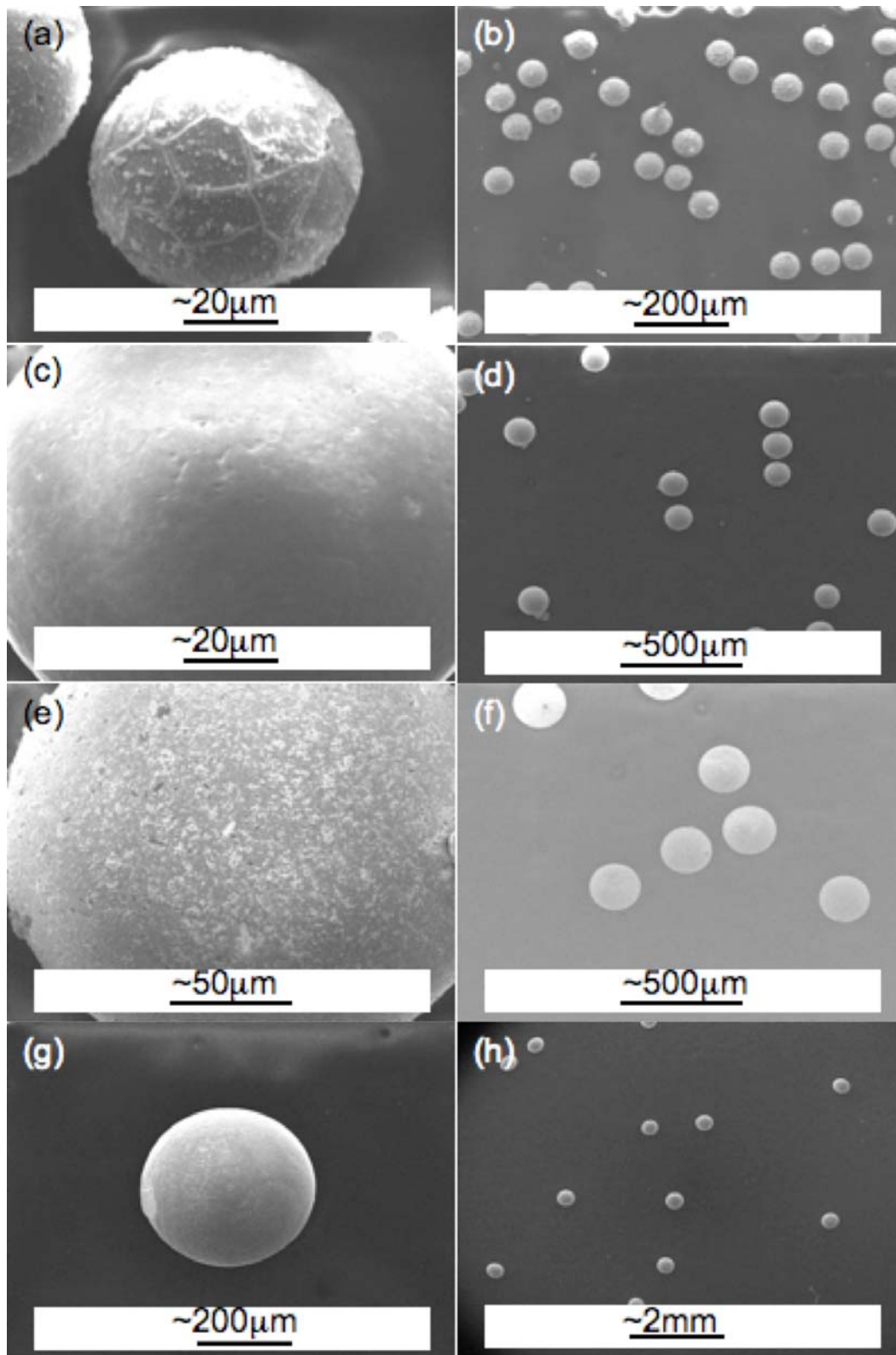


Figure 9: SEM photos of the 53 (a and b), 102 (c and d), 196 (e and f), and 305 (g and h) micron particles. The pictures were taken at the University of Michigan Electron Microbeam Analysis Laboratory (EMAL).

The photos in Figure 9 confirm the tolerances that were reported by the manufacturers and that the particles are very close to spherical. But, it should be noted that the surfaces of the particles are not perfectly smooth, which is assumed in the model. The silver coated glass particles appear to have much rougher surfaces than the 95Sn/5Sb particles. The effects of the rough particle surfaces are addressed in more detail in a later section.

The experiment was performed with two different electrode materials, gold and platinum. These materials were chosen because they do not oxidize when exposed to the atmosphere unlike most other metals. When manufacturing the electrodes, the two biggest concerns were controlling the surface flatness and the surface roughness. Controlling surface flatness is important for reducing the error in the applied electric field since a warped surface can lead to varying electric field strengths at the electrode surface. The surface roughness is important because the model for the van der Waals adhesion force assumes that the surface of the electrode is perfectly smooth.

To minimize the surface roughness and control the flatness, the electrodes were fabricated using plasma vapor deposition of the metals onto glass wafers. All depositions were performed using the EnerJet Evaporator at the Lurie Nanofabrication Facility (LNF) located at the University of Michigan. The gold electrodes were fabricated by depositing 300 nm of gold on top of a 30 nm adhesion layer of chromium, and the platinum electrodes were fabricated by depositing 100 nm of platinum on top of a 10 nm adhesion layer of titanium. Figure 10 is a picture of one of the gold electrodes.



Figure 10: Picture of a gold electrode deposited on a glass wafer.

The electrodes are circular with 50 mm diameters and were deposited onto 100 mm glass wafers. A thin tail of metal stretches from the electrode and wraps around the wafer to provide an electrical connection on the reverse side.

An atomic force microscope (AFM) was used to measure the surface roughness of both the gold and platinum electrodes, and both were found to have a surface roughness on the order of 20 nm. The effects of the electrode surface roughness are presented in an upcoming section.

The experiment was performed in the Ultra High Vacuum (UHV) chamber at the Space Electrodynamic and Tether Systems (SETS) laboratory at the University of Michigan, which is pumped by a mechanical roughing pump and a turbo pump and has an ultimate pressure on the order of 10^{-9} Torr. Each experiment was performed at a pressure less 40 nTorr to prevent arcing within the electrode gap.

B. Experimental Results

Before presenting the experimental results, it is important to remind the reader that the Lifshitz-van der Waals constant from Equation (2) is not well known for most material combinations. Further, in the cases of reported values, many authors are not in agreement.¹³ Therefore, this paper does not assume any values for the Lifshitz-van der Waals constant when analyzing the results. Instead, values for the Lifshitz-van der Waals constant that best fit the experimental results are evaluated and used for comparison between the test

cases. The threshold electric field for particle removal is defined as the field strength at which 50% of the particles in contact with the source electrode are removed.

Figure 11 and Figure 12 are plots showing the measured electric fields required for particle removal for all eight cases tested. Each plot shows the results for all four particle sizes tested against one of the two electrode materials. The solid black dots represent the electric field strength at which 50% of the particles tested were removed. The upper and lower dashes represent the electric field strengths at which 33% and 67% of the particles were removed, respectively. Each test case measured the threshold electric field of several hundred particles over several experimental runs, with the exception of the 305 μm particles, which used less than ten particles per experimental run due to the tendency of the particles to roll off of the electrode during setup. The error in the electrode gap is the largest source of error in the electric fields, which is estimated to be approximately 5%.

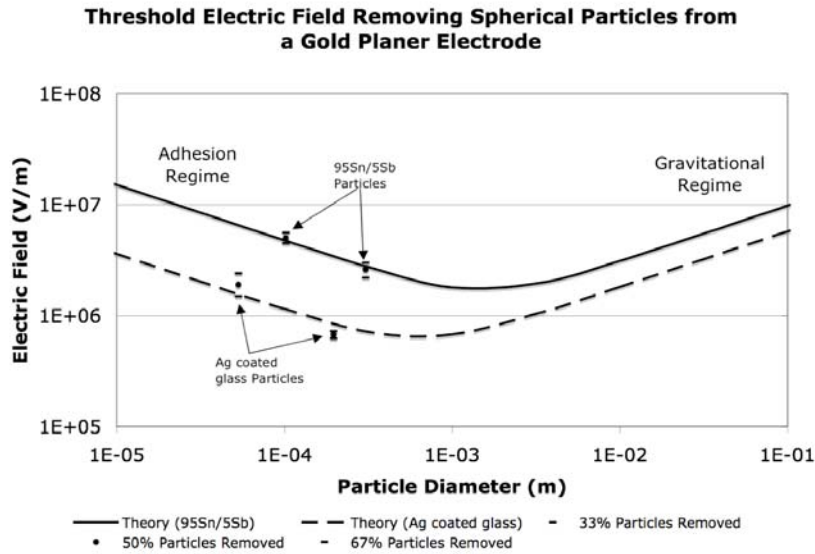


Figure 11: Measured threshold electric fields for removal of spherical particles from a gold planar electrode when in the adhesion dominant regime.

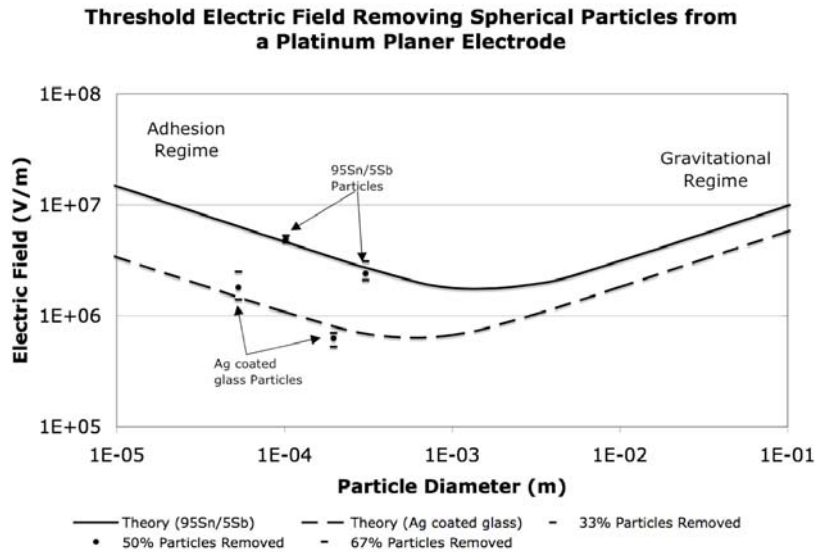


Figure 12: Measured threshold electric fields for removal of spherical particles from a platinum planar electrode when in the adhesion dominant regime.

The experimental data is plotted against the theoretical threshold electric fields when using the Lifshitz-van der Waals constants evaluated to provide the best fit. Table 2 lists the evaluated Lifshitz-van der Waals constants for the four material combinations used in Figure 11 and Figure 12, and are all on the order of the expected range of 0.6 to 9 eV. As predicted by the model, the threshold electric fields required for particle removal increase as the particle size decreases for each material combination. But, note the large variation in the threshold electric fields between the two particle materials. This variation may be a result of a difference between the actual Lifshitz-van der Waals constants, a difference between the materials' surface roughness, and/or particle deformation, which are discussed in the upcoming sections. Also, note that changing the electrode material from gold to platinum has very little effect on particle adhesion.

Material Combination	Lifshitz Constant (eV)
95Sn/5Sb – Au	4
95Sn/5Sb – Pt	4
Ag coated glass – Au	0.2
Ag coated glass – Pt	0.2

Table 2: Lifshitz-van der Waals constants evaluated to match experimental data for all material combinations tested.

The spread of the threshold electric field required for particle removal is larger than expected. Figure 13 shows the percentage of particles removed as a function of the applied electric field for all eight test cases.

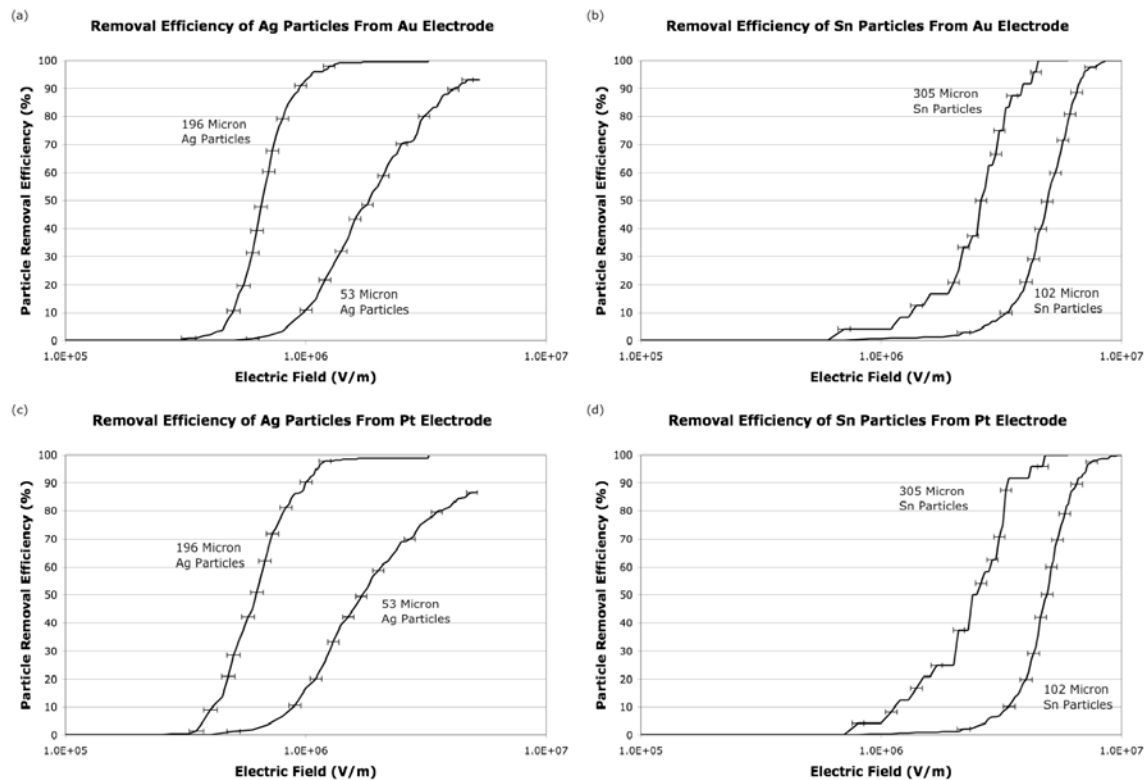


Figure 13: Plots of the particle removal efficiency as a function of applied electric field for all eight test cases.

To complement Figure 13, Table 3 lists the median threshold electric field strength for particle removal along with the electric field strengths required to remove 15%, 33%, 67%, and 85% of the particles.

Particle Size and Materials	Required Electric Field to Remove Stated Percentage of Particles				
	15% (MV/m)	33% (MV/m)	50% (MV/m)	67% (MV/m)	85% (MV/m)
305 μm Sn on Au	1.6	2.2	2.6	3.0	3.5
305 μm Sn on Pt	1.4	2.1	2.4	3.1	3.3
196 μm Ag on Au	0.53	0.63	0.68	0.73	0.85
196 μm Ag on Pt	0.48	0.53	0.63	0.70	0.88
102 μm Sn on Au	3.7	4.5	5.0	5.6	6.3
102 μm Sn on Pt	3.7	4.6	4.9	5.3	6.1
53 μm Ag on Au	1.1	1.5	1.9	2.4	3.6
53 μm Ag on Pt	1.0	1.4	1.8	2.5	4.5

Table 3: Threshold electric fields required to remove 15%, 33%, 50%, 67%, and 85% of the particles.

Potential reasons for the spread in the electric field required for particle removal are presented in the upcoming sections, which include the spread in particle size, the particle and electrode surface roughness, and the surface deformation.

C. Variables of the Experiment

While the measured threshold electric fields trend as predicted by the model for each material combination, the evaluated Lifshitz-van der Waals constants for the two particle materials are quite different. The evaluated Lifshitz-van der Waals constants may be reasonable measurements of the actual values, or the difference may also be a result of uncontrolled variables in the experiment. In addition, the spread of the electric fields required for the removal of all the particles is quite large, which may also result from uncontrolled variables in the experiment. This section examines three variables in the experiment.

The first experimental variable to consider is the spread in particle size, which may contribute to the spread in the electric fields required for particle removal. Using the tolerances on the particle diameters given in Table 1 and the predicted threshold electric field from Equation (6), the expected electric field spread can be calculated. Table 4 lists the approximate expected electric field spread resulting from the particle size spread along with the measured spread to remove 15%-85% and 33%-67% of the particles.

Particle Diameter (μm)	Electrode Material	Theoretical Spread (MV/m)	33%-67% Measured Spread (MV/m)	15%-85% Measured Spread (MV/m)
305	Au	0.09	0.80	1.9
305	Pt		1.0	1.9
196	Au	0.07	0.10	0.33
196	Pt		0.18	0.40
102	Au	0.48	1.1	2.6
102	Pt		0.70	2.4
53	Au	0.13	0.90	2.5
53	Pt		1.1	3.5

Table 4: The estimated spread in the threshold electric field due to the spread in particle size and the measured threshold electric field spread.

The calculations in Table 4 suggest that the spread in particle size can lead to a spread in the electric field, but not enough to account for the entire spread in the experimental data.

The second experimental variable is possible deformation of the particle and/or the source electrode by compression. The model presented in Equation (2) assumes that the particle is a perfect sphere and that the electrode is a perfect plane, but, due to defects in the particle and/or the electrode, this is most likely not the case. The compression of either the particle or the electrode leads to a contact area between the two greater

than just the point contact that is assumed. An increase in the contact area leads to an increase in the adhesion force.

Approximating the change in the adhesion force due to the deformation of the particle and/or the electrode is not straightforward because the exact geometry after deformation has occurred is unknown and can be quite complex. To approximate the change in the adhesion force resulting from deformation, all of the deformation is assumed to be at the bottom of the particle. Using Equation (1), the adhesion force with a compressed particle is calculated to be a function of the contact area radius, r_c .⁶

$$F_{vdw,def} \approx \frac{h}{8\pi z^2} \left(r + \frac{r_c^2}{z} \right) \quad (7)$$

Assuming that the electric force on the particle does not change significantly if the particle experiences a small deformation, which is appropriate as long as the deformation occurs at the bottom of the particle, the new threshold electric field is calculated by modifying Equation (6) and assuming that the particle is in the adhesion dominant regime.

$$E_{thresh,def} \approx \sqrt{\left(\frac{1}{r} + \frac{r_c^2}{r^2 z} \right) \frac{h}{z^2 \epsilon}} (0.0023) \quad (8)$$

The deformation of the particle may lead to an error in the evaluated values of the Lifshitz-van der Waals constant from the experimental results. Figure 14 is a plot of the percent error in the evaluated Lifshitz-van der Waals constants as a function of percent deformation of the particle for all four particles tested. The deformation of the particle is defined as the ratio of the contact area radius to the particle radius, $r_c:r$.

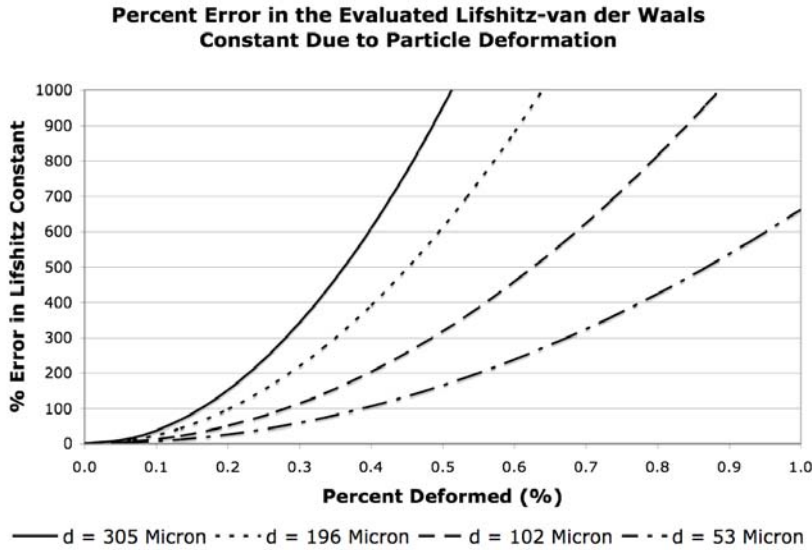


Figure 14: The estimated percent error of the evaluated Lifshitz-van der Waals constants due to deformation of the particle.

Figure 14 shows that just a slight deformation of the particle can lead to a very large error in the evaluated Lifshitz-van der Waals constant, which could be a large error in the evaluated values listed in Table 2.

In addition to increasing the error in the evaluated values for the Lifshitz-van der Waals constant, the particle deformation may also be a source of the spread in the electric field required to remove all the particles. Figure 15 plots the approximate expected threshold electric field spread resulting from particle

deformation for all 4 particle sizes tested. The figure assumes Lifshitz-van der Waals constants of 4 and 0.2 eV for the 95Sn/5Sb and Ag particles, respectively.

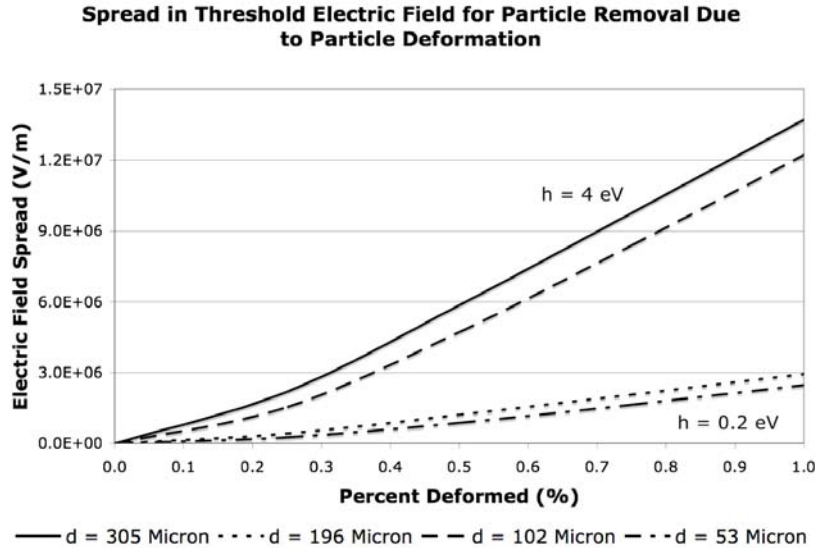


Figure 15: The estimated spread in the threshold electric field due to deformation of the particle.

Comparing the theoretical spread in the electric field with the measured spread from Table 3, it is very possible that a small deformation could make significant contributions.

The final experimental variable that may potentially influence the electric field spread that is discussed in this paper is the surface roughness of both the particle and the electrode surface. The surface roughness of the materials in contact can lead to an increase or decrease in the adhesion van der Waals force depending on their relative roughness and alignment.¹⁴ Due to the complexity and large number of variations of surface roughness and alignments, it is not possible to provide a general relationship between the adhesion force and the materials surface roughness. Only in the case when the exact geometry of the two surfaces is known, can Equation (1) be integrated to find the adhesion force.

Figure 16 illustrates four possible surface orientations between the electrode surface and the particle. Note that the examples discussed here are not all inclusive and there exist many other possible surface orientations that may lead to a change in the adhesion force.

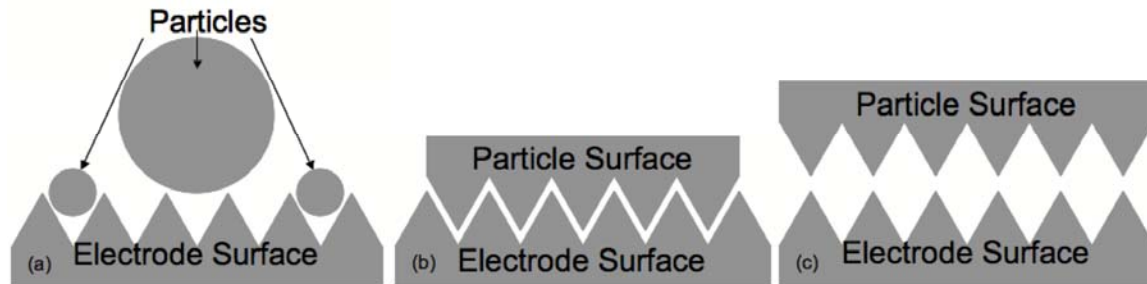


Figure 16: Possible electrode and particle surface orientations.

Sketch (a) from Figure 16 illustrates two possible situations. First, it is possible that the particles are much smaller than the surface roughness of the source electrode. In this case, the particles may fit between the peaks and valleys of the electrode, which increases the contact area and increases the adhesion force. Second, it is possible that the particles are much larger than the surface roughness and sit on the peaks of the electrode, which decreases the contact area and decreases the adhesion force. Picture (b) illustrates a case when the surface roughness of the particle and the electrode are approximately the same and are aligned so that the peaks of the particle fit into the valleys of the electrode. Again, this increases the

contact area and the adhesion force. Picture (c) illustrates a case when the surface roughness of the particle and the electrode are approximately the same and are unaligned so that the peaks of the particle and electrode are touching. This decreases the contact area and the adhesion force.

As stated earlier, there exist many other possible orientations between the particle and electrode surfaces, and their effects on the adhesion force can be determined by understanding how the contact area changes. Since the surface roughness affects the adhesion force by changing the contact area, it is reasonable to expect that the error in the evaluated values for the Lifshitz-van der Waals constants and the resulting spread of the electric field required for particle removal are on the same order of magnitude as the case of particle deformation.

Figure 9 is a set of SEM photographs of the particles used for this paper, and shows that the particles all have surface defects on the order of what appears to be microns, but note that the defects on the silver coated glass spheres are much larger than on the 95Sn/5Sb particles. Both electrode surfaces have a surface roughness on the order of 20 nm.

Based on the analysis presented in this subsection, it is possible that the evaluated values for the Lifshitz-van der Waals constants deviate from the actual values due to the deformation of the particles and/or the electrode and the surface roughness of particles and the electrode. The large spread in the electric field required for particle removal is most likely contributed to significantly by the same two experimental variables, and to a lesser extent, the spread in particle size.

D. Lifshitz-van der Waals Constant

As discussed in a previous section, the Lifshitz-van der Waals constant is used to calculate the van der Waals force between two macroscopic materials and is a measure of the energy of the van der Waals interaction.⁵ For materials in atmosphere or vacuum, its value generally ranges from 0.6 to 9.0 eV and is obtained using dielectric spectroscopy.^{15,16}

Calculating the Lifshitz-van der Waals constant is beyond the scope of this paper, but is known to be difficult due to the lack of available optical data.¹³ Table 5 lists the expected ranges of the Lifshitz-van der Waals constants for a couple of the experimental material combinations using published values.^{6,13} For comparison, the evaluated values of the Lifshitz-van der Waals constants from the experimental results are included in the table.

Materials in Contact	Predicted Lifshitz-van der Waals Constant (eV)	Evaluated Lifshitz-van der Waals constant (eV)
Au - 95Sn/5Sb	6.6-8.2	4
Au - Ag	5.8-10.3	0.2

Table 5: List of ranges of the expected values of the Lifshitz-van der Waals constant for select test cases compared with the evaluated values.

Note that the evaluated Lifshitz-van der Waals constants lay outside the range of predicted values for the given material properties, but are close to the expected range for all material combinations. There is possible error in the evaluated values as discussed in the previous subsection. But, according to Visser:¹³

“Comparison of the theoretically calculated Lifshitz-van der Waals/Hamaker constants with those derived from experiments show that in a large number of cases the values from colloid chemistry and surface tension measurements deviate substantially from the theoretically calculated ones. This finding is a clear indication that the interpretations used for their calculation are based on incomplete theories.”

4. Overcoming the Cohesion Force Using Ultra-Fine Particle Sieves

This section investigates the feasibility of overcoming the cohesion force by using a method of transporting the dry particles through an ultra-fine sieve to separate the clumped powder into individually isolated particles prior to charging and acceleration as presented in the introduction. The details of the design and optimization of the sieving particle delivery system is beyond the scope of this paper. Instead, results from a proof-of-concept experiment are presented with the goal of demonstrating the feasibility of this delivery system. The main goals of the proof-of concept experiment are to demonstrate the

functionality of the first prototype by confirming that particles are charged, accelerated and ejected individually.

A. Experimental Setup

To experimentally investigate the method of delivering individual dry spherical particles through an ultra-fine sieve prior to charging and accelerating, the prototype shown in Figure 17 was constructed using a stainless steel cloth with orifice diameters of approximately $20\ \mu\text{m}$ and was tested with hollow aluminum spherical particles with diameters ranging from $5\ \mu\text{m}$ to $20\ \mu\text{m}$. A cylindrical acrylic plunger is mounted beneath the sieve and the space between the plunger and the sieve acts as the particle reservoir. The weight of the sieving system on the particle reservoir, along with a mechanical vibrational source (not pictured), forces the particles through the sieve. Mounted on the topside of the sieve is the charging grid, which is at a distance of approximately $7.5\ \text{mm}$ from the sieve surface and has a single $5\ \text{mm}$ orifice to allow the passage of particles. Above the charging grid is the collection anode used to collect all ejected particles.



Figure 17: First generation prototype using sieving delivery method.

The sieve is electrically connected to ground while the charging grid and the collection anode are biased positive using a high voltage power supply to generate the charging electric field. Note that this prototype does not include any additional accelerating grids, but stacking additional grids above the charging grid is possible. To verify that the particles were ejected individually and not clumped in groups, ejected particles were collected on glass slides placed just above the orifice in the charging grid and imaged using a scanning electron microscope (SEM).

B. Experimental Results

Figure 18 is an SEM image of a glass slide after bombardment of the aluminum particles from the prototype for approximately one second.

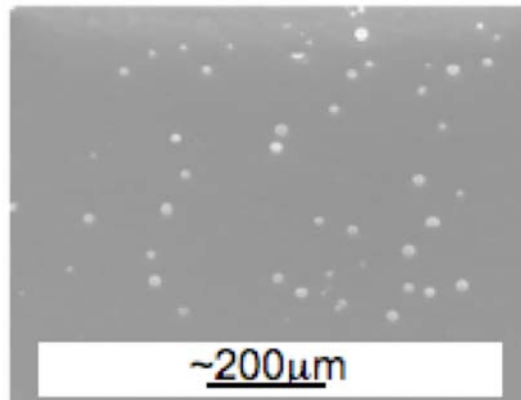


Figure 18: An SEM image showing aluminum particles collected on a glass slide after bombardment.

Figure 18 shows that most of the particles collected by the slide are individual particles, which supports the theory that the particles are ejected individually. The proof-of-concept experimental results presented in this paper suggest that the sieving delivery method is capable of ejecting individually isolated particles continuously. Additional methods to verify this are currently under development and will be published when available.

5. Conclusion

The effects of the adhesion and cohesion forces on the no-liquid configuration were presented along with potential methods of overcoming them. For conducting particles in a dry environment, the dominant adhesion and cohesion force is the van der Waals force, which scales directly with the particle size. Overcoming the adhesion force by removing spherical conducting particles from a planar source electrode by way of applied electric fields was investigated. The electric force responsible for particle removal scales directly with the square of the particle size while the adhesion force scales directly with the particle size. This suggests that as the particle size decreases, the required electric field for removal increases. The models developed predict that particles with diameters down to hundreds or even tens of nanometers can be removed from a planar electrode. Note that there may exist methods of reducing the required electrical force, such as the use of mechanical vibration, which is presented in a companion paper.¹⁷

To investigate the particle removal model, eight test cases, involving 4 particle sizes and 2 electrode materials, were studied. The tests agreed reasonably well with the model when using values of the Lifshitz-van der Waals constants close to the expected ranges for all materials. But, the values evaluated from the experimental data disagree with published values for the specific material combinations. Note that many authors are not in agreement on the published values. In addition, the spread in the electric fields required to remove particles was large. The possible error in the Lifshitz-van der Waals constants and the spread of the electric fields may be attributed primarily to the surface roughness and deformation of both the particles and the electrode.

Overcoming the cohesion force by delivering the particles through an ultra-fine sieve was investigated by performing a simple proof-of-concept experiment, which suggests that it is a viable method. Further testing is required, but the initial results are promising.

Acknowledgments

This project is funded by an Air Force Office of Scientific Research grant (FA9550-07-C-0144, managed by Dr. Mitat Birkan).

References

- ¹ L. Musinski, T. Liu, B. Gilchrist, A. Gallimore, M. Keidar. "Scalable Flat-Panel Nano-Particle MEMS/NEMS Thruster." International Electric Propulsion Conference (IEPC), October 31 – November 4, 2005.
- ² Liu, T., Musinski, L., Patel, P., Gallimore, A., Gilchrist, B., and Keidar, M., "Nanoparticle Electric Propulsion for Space Exploration." Space Technology and Applications International Forum (STAIF), Albuquerque, NM, February 11-15, 2007.
- ³ Behan, Niall, "Nanomedicine and Drug delivery at the University of Limerick," The University of Limerick. <http://www.ul.ie/elements/Issue4/beh.htm>
- ⁴ Musinski, L., Liu, T., Gilchrist, B., Gallimore, A., and Keidar, M., "Experimental Results and Modeling Advances in the Study of Nanoparticle Field Extraction Thruster." AIAA-2007-5254, 43rd AIAA/ASME/SAE/ASEE Joint Propulsion Conference & Exhibit, Cincinnati, OH, July 8-11, 2007.
- ⁵ Podczek, F., "Particle-Particle Adhesion in Pharmaceutical Powder Handling." Imperial College Press, London, 1998.
- ⁶ Bowling, R. "An Analysis of Particle Adhesion on Semiconductor Surfaces." J. Electrochem. Soc.: Solid-State Science and Technology. Sept, 1085.
- ⁷ Curran, C., Watkins, K., Lee, J. "Shock Pressure Measurements for the Removal of Particles of Submicron Dimensions from Silicone Wafers." 21st International Congress on Applications of Lasers and Electro-Optics, 2002.
- ⁸ Leider, P., Olapinski, M., Mosbacher, M., Boneberg, J. "Nanoparticle Adhesion and Removal Studied by Pulsed Laser Irradiation." High-Power Laser Ablation. Vol 6261. 2006.
- ⁹ Felici, N. Rev. Gen. Elect., 75, pp. 1145-1160, 1966.
- ¹⁰ Tobazeon, R. "Electrohydrodynamic Behavior of Single Spherical or Cylindrical Conducting Particles in an Insulating Liquid Subjected to a Uniform DC Field." Journal of Physics, 29, 2595-2608, 1996.
- ¹¹ Deline, C., Goldberg, H., Morris, D., Ramos, R. "Field Emission Cathodes Used in the FEGI Get Away Special Shutter Mission." AIAA-2004-3498, 40th AIAA/ASME/SAE/ASEE Joint Propulsion Conference and Exhibit, Fort Lauderdale, FL, July 11-14, 2004.
- ¹² Dupont Technical Information "Dupont™, Kapton® Insulation Substrate," Dupont High Performance Materials, 2001.
- ¹³ Visser, J., "On Hamaker Constants: A Comparison Between Hamaker Constants and Lifshitz-Van Der Waals Constants." Advances in Colloid and Interface Science. 1972. Pp 331-363.
- ¹⁴ Rabinovich, Y., Adler, J., Ata, A., Singh, R., Moudgil, B. "Adhesion Between Nanoscale Rough Surfaces." Journal of Colloid and Interface Science. 232, 17-24, 2000.
- ¹⁵ Krupp, H., "Particle Adhesion Theory and Experiment." Advan. Colloid Interface Sci. 1, 111-239, 1967.
- ¹⁶ Anandarajah, A., Chen, J. "Single Correction Function for Computing Retarded Van der Waals Attraction." Journal of Colloid and Interface Science. 176, 293-300, 1995.
- ¹⁷ Liu, T., Drenkow, B., Musinski, L., Gallimore, A., Gilchrist, B., Millunchick, J., Morris, D., Doan, A., Munski, J., Muldoon, A., "Developmental Progress of the Nanoparticle Field Extraction Thruster." AIAA-2008-5096, 44th AIAA/ASME/SAE/ASEE Joint Propulsion Conference & Exhibit, Hartford, CT, July 21-23, 2008.